PIV MEASUREMENTS OF CONFINED SWIRLING FLOW

Kristofer Midgley, Adrian Spencer, James J McGuirk
Department of Aeronautical and Automotive Engineering, Loughborough University
Loughborough, Leicestershire LE11 3TU, UK

ABSTRACT

The paper reports an experimental study of the highly swirling flowfield typical of a gas-turbine fuel injector. An isothermal (water flow) experiment is conducted to measure the time-mean and instantaneous aerodynamic behaviour. The PIV technique is used for data gathering. Validation tests are carried out with various fields of views to ensure that the PIV interrogation window size is small enough in comparison with local turbulent length scales to avoid loss of turbulence information during the cross-correlation evaluation. The time-averaged flowfield displays many classical characteristics of high swirl number shear flows. Interesting features are revealed on examination of the instantaneous data. These include a rotating four-vortex pattern issuing from the swirler stream, and a precessing vortex core. Detailed information is presented on these unsteady features so that the data set represents a challenging test case for LES methods.

INTRODUCTION

Swirling flow is used in gas-turbine combustor fuel injectors to provide a means of manipulating primary zone aerodynamics and controlling fuel/air mixing. Swirl-induced recirculation zones are a common feature of many designs, and intense swirl provides improved mixing performance. Interest has also focussed on the unsteady features of high swirl flows, for example the existence of a precessing vortex core (PVC) (Yazdabadi et al, 1994 and Anacleto et al, 2001), or the vortex breakdown phenomenon (Brooke-Benjamin, 1962, Leibovich, 1978, Wang and Rusak, 1997). The existence, and the precise frequency, of a PVC introduce a 3D time-dependent coherent flow structure into the mixing region of combustors. Vortex breakdown in high swirl flows has been studied for many years, since it was first explained (Brooke-Benjamin, 1962) as a transition (analogous to a hydraulic jump) between a supercritical flow state (which can not sustain disturbances in the form of axisymmetric waves) and a subcritical state (which allows disturbances to propagate and grow). The transition between the states takes the form of a stagnation region, whose formation is important in terms of creating a flame stabilising zone in combustors. In CFD calculations of such flows, the subcritical nature of the flow implies strong sensitivity to downstream boundary conditions. The significance of breakdown or precession phenomena is that they are difficult to simulate with statistical turbulence models. The low emissions performance of swirl-dominated fuel injectors, depends strongly on avoiding regions of instability that influence mixing and, under combusting conditions, can cause large, possibly damaging pressure oscillations.

The importance of these swirl-induced phenomena to the aerodynamic design of combustion systems has lead to recent studies examining the ability of the Large Eddy Simulation (LES) approach to capture not only the time-averaged flow pattern, but also time-dependent features (Tang et al, 2002, Stone and Menon, 2002). Experimental data to validate such predictions is, however, relatively scarce. The purpose of the present work was therefore to design an experiment containing a confined high swirl flow that was simplified but generically representative of the flow-field created by aero-engine combustor fuel-injector systems. The measurements should form a benchmark validation test case for LES methods by providing details of the instantaneous flow structure. To this end, Particle Image Velocimetry (PIV) has been used to deliver 2D spatial resolution of flow structures and their unsteady dynamics. An isothermal experiment was performed to allow emphasis to be placed on the unsteady aerodynamic phenomena. To ease seeding and other instrumentation problems, a water flow experiment was selected. This is described in detail in the following section, followed by information on the PIV system and the checks for statistical and resolution accuracy of the turbulence data. The paper presents a selection of the time-averaged data acquired (mean and turbulence statistics), as well as instantaneous and time-resolved information such as spectra and frequency content of unsteady flow structures

EXPERIMENTAL FACILITY

The experimental rig is shown in Fig. 1. The rig used a single constant head supply to feed two vertically oriented, concentrically mounted tubes. The fuel injector consisted of a swirl stream (radially-fed swirler containing 12 tangential 30° slots) and a central round jet simulating a fuel stream. Both swirl and jet streams discharged into a larger diameter cylindrical duct (D = 140 mm). The diameter of the duct relative to the fuel injector was chosen to be typical of the level of confinement found in aero-engine combustors. A valve in the water return circuit from test section exit to the sump tank controlled the total flow rate. An upstream throttle plate controlled the flow split between swirl and jet

streams. The flow rate was set to ensure the Reynolds number was sufficiently high to guarantee fully turbulent flow. A central axisymmetric blockage was introduced downstream to prevent problems with an elongated central recirculation zone, and provide a controlled exit boundary condition from the test section. The test section was surrounded by a square section water jacket to minimise refraction and distortion of the laser light sheet by curved surfaces. In addition to the light sheet illuminating an axial-radial (x-r) plane, a window was created in the downstream to allow the camera to view an r-θ oriented light sheet. The distance of the downstream blockage from the fuel injector exit was varied in preliminary tests. The final position, to provide sufficient blockage without changing the flow in the immediate vicinity of the fuel injector, was 160mm.

The fuel injector studied is shown in Fig. 2. The radially fed swirler produced an annular swirl stream (outer diameter D_s = 37.63mm) at fuel injector exit. The inner diameter of the annulus was formed by the outer wall of a central jet nozzle (inner diameter D_j = 5.4mm). The test conditions corresponded to swirl and jet Reynolds numbers of $8x10^4$ and $2.63x10^4$ respectively. Re is here defined using D_s and D_j and velocities based on geometrical exit areas: U_j = 4.88m/s, U_s = 2.13m/s. Note, however, that the discharge coefficient of the swirl passage was measured to be 0.5, so the peak velocity in the swirl stream was about $1.5U_s$. Tests to study Reynolds number effects were carried out, but no discernable differences could be measured in non-dimensional mean or turbulence profiles. Tests without the jet stream examined the extent to which this influenced the flow pattern.

INSTRUMENTATION

The PIV instrument comprised a LaVision system with a twin Nd:Yag laser generating a 1mm thick light sheet via spherical and cylindrical lenses, and a Kodak Megaplus ES 1.0 camera with 1024x1024 pixel resolution, running at 15Hz. Laser/camera synchronisation, image acquisition, and data processing using the cross-correlation technique were controlled by Davis software running on a dual processor Pentium III PC. 20μm Polyamide particles (almost neutrally buoyant in water) were used as light scattering particles. The PIV set-up was selected following the recommendations of Adrian (1991). Laser power and optical system/data collection parameters were optimised so that the particle image size corresponded to 2 pixels and the particle shift was approximately 1/4 of the PIV interrogation window used for cross-correlation evaluation. In most data collected there were around 10 particle pairs per interrogation window, although sometimes there were less than this. The interrogation cell used a deformed multi-pass grid (LaVision, 2000) of initial size 64x66 pixels, reducing to a final size of 32x32 pixels (with 50% overlap). The inter-frame delay time was around 500μs for the large field of view (FoV) images, and 20-50μs for the smallest FoV. This choice minimised out of plane data loss and maximised the in-plane displacement, which was typically from 3-8 pixels.

To provide a separate crosscheck on the PIV data collected, an LDA system was also used. This comprised a 20mw He-Ne laser with Dantec optics, frequency shifting and photomultiplier, and a TSI IFA550 processor. Data were usually taken at a fixed sampling rate of 1kHz and blocks of data of up to 25,000 points were used to allow time-histories, auto-correlations and spectra to be evaluated.

DATA VALIDATION

The axial-radial (x-r) plane of the test section was initially captured using a large FOV of $160x160mm^2$. This allowed illumination of the entire flowfield between fuel injector and downstream blockage in a single view, but resulted in an interrogation cell size of $5x5mm^2$. Fig. 3 shows a time-averaged axial velocity contour map obtained in this way. The central jet penetration, swirler "cone angle", corner and central recirculation zones are all clearly visible. To obtain converged, stationary time-averages, a large enough number of statistically independent samples must be gathered. The maximum number of instantaneous velocity vector images that could be stored in the PC memory was 650. The statistical convergence of this data was examined. Fig. 4 shows this for the time-mean axial velocity at a point in the swirl stream shear layer (x/D_s = 0.26, r/D_s = 0.35 - origin of the x-r system on the duct centre-line at fuel injector exit). Randomly chosen blocks of between 5 and 650 data points were used to obtain the mean. The convergence of the time-averaged value as the block size increases agreed well with standard error estimates for a 95% confidence level; similar results were obtained for the turbulence normal stresses. Hence, it is believed that 650 PIV 'frames' are sufficient to obtain time-mean values

Although the time-averaged picture in this large FOV is quite close to symmetric, deviations can be seen due to insufficient spatial resolution. In addition, it is known that the turbulence energy measured using the PIV technique, even if statistically converged, can be in error if the size of the interrogation cell is not small compared to the local integral length scale. Host-Madsen and Nielson (1998) have analysed this problem. It is related to the loss of turbulence information due to filtering applied to the set of particle pairs contained within a PIV interrogation cell. If at least 90% of the contribution to turbulence energy of the fluctuating motions is to be captured, Host-Madsen and Nielson (1998) recommended that the interrogation window should be no larger than about 1/5 of the local integral scale. Hollis et al (2001) found that this estimate agreed very well with their PIV measurements of flow over a wall-mounted obstacle, where the turbulent length scale was deduced from LDA measurements. Since the integral scale is unknown when the measurements are performed, and in any case varies across the flowfield, the best data validation that can be done is either to take measurements of the same flow region with various FoVs (reducing in size), or to compare the turbulence data obtained from the PIV instrument with LDA measurements, which do not suffer from this problem. Both techniques have been adopted in the present work.

Three FoVs have been used in the validation process. The large FoV has been mentioned above (Fig. 3 $160x160mm^2$, $5x5mm^2$ interrogation cells). An intermediate FOV was selected which allowed the whole flowfield to be captured in 4 images ($80x80mm^2$, $2.5x2.5mm^2$ cells). Fig. 3 shows the 4 intermediate FoVs (regions a-d), and region a is shown in Fig. 5. Finally, small FOV data sets were gathered ($20x20mm^2$, $0.63x0.63mm^2$ cells) in order to capture

velocity information as accurately as possible. Fig. 5 indicates the 6 regions selected for study in this way.

Fig. 6 presents a comparison between intermediate and small FoVs for the axial mean velocity and associated r.m.s. level on a profile across the central jet (6a) and the swirl flow (6b) at x = 10mm. The agreement between the two PIV data sets is good across the whole radial profile. Similarly, Fig. 7 compares two PIV FoV sizes for r-θ plane measurements (slightly different FoVs to those quoted above) and shows swirl velocity and r.m.s. level at x = 40mm. LDA data for the same profile are included and again good agreement is obtained. These tests are considered sufficient to provide thorough validation for both first and second moments of the PIV data presented below.

RESULTS

The swirl number S evaluated from measured axial and swirl profiles at fuel injector exit was 0.85. At this level of S, the mean flowfield characteristics displayed in Figs. 3 and 5 are of the classical, expected type. A swirling shear layer with an included angle of 60^0 is formed and impinges on the outer duct wall forming a corner recirculation region. The central recirculation zone expected at this swirl number is formed, but interacts with and is modified by both the central jet (which penetrates to about x/D_s =1.0) and the separation zone of the downstream blockage. The swirl fluid forms a high velocity wall jet after impingement and exits the duct via the downstream annular exit. The flow structure in the near field of the fuel injector is displayed in more detail in Figs 6 and 7. Figs 6a and 6b indicate the shape of the radial profile of axial velocity at x=10mm across jet and swirl streams. A backflow zone is trapped between swirl and jet streams at this location, creating a high shear region. This leads to high turbulence production in the shear zones. Interestingly, only the inner side of the swirl shear layer displays high turbulence levels, and this is discussed further below. The shape of the swirl profile at x=40mm (Fig. 7) does not display a clear Rankine vortex shape, but shows two regions of steep, but different swirl gradient, the inner gradient is shallower as this contains both fluid from the swirl stream and non-swirling fluid from the jet. The circumferential r.m.s at this station is less than in the axial component (not shown), indicating high anisotropy. One important feature is the peak in circumferential r.m.s on the centre-line. This is evidence of a precessing vortex core, and the high turbulence level measured by long-time-averaged PIV data is not entirely 'true' turbulence, as it contains a contribution from a coherent periodic motion (more details below). The strength of the precession is strongly affected by the central jet. This tends to stabilise both the swirl shear layer, and reduce the vortex precession. Evidence for this is given in Fig. 8, which compares swirl profile information at x=40mm with and without the central jet flow. Without the jet, a very strong gradient of mean swirl is formed near the centre-line, and this enhances the precession, leading to extremely high circumferential r.m.s. levels.

Time-averaged data are informative, but do not reveal the detailed flow characteristics completely, particularly of unsteady phenomena such as a precessing vortex core. For this, instantaneous vector maps may be examined. Fig. 9 shows an instantaneous image of the swirl/jet shear layer in the x-r plane. Vortex structures are clearly visible on the inner edge of the shear layer. To explore the origin of these structures, instantaneous vector maps were gathered in r-θ planes, starting at x=-1mm, i.e. just upstream of the fuel injector exit plane. Fig. 10 shows one selected view. It is clear that streamwise vortices are being formed in the annular swirl duct. Four vortices are visible, 2 strong and 2 much weaker. The origin of these is thought to be a vortex breakdown phenomenon in the swirl stream as it flows through the annular duct. Inside the fuel injector, there is significant area variation and a corner discontinuity can also be seen (Fig. 2). Further work is needed to confirm this hypothesis, for example, it is unclear why 4 vortices should be formed (there are 12 swirler slots).

The picture in Fig. 10 is of course a single time snapshot. The vortex pattern rotates with the swirl. The frequency of this rotation cannot readily be identified from the PIV data as this has a time resolution of only 15Hz. LDA data were taken at selected points in the swirl shear layer. Since these data were taken at a sampling rate of 1kHz, frequencies up to 500Hz can be identified. Fig. 11 shows a power spectral density (PSD) deduced from a time-history of the circumferential velocity at the point: x/D_s = 0.03, r/D_s = 0.19. This data indicate that strongly periodic motions are present. The strongest peak is at 74.6Hz, with a second weaker (but still very energetic) peak at 153.6Hz, close to a harmonic of the first frequency. The mean swirl velocity at swirler exit at the radius of the vortices seen in Fig. 10 was 2.3 m/s. Combination of the circumferential path length and this velocity leads to an implied rotation rate of 41Hz. Since there are 2 strongly coherent vortices, the 76 Hz frequency corresponds closely to the rotation of this 2-vortex pattern past a fixed point. The rotation of the 4-vortex pattern gives rise to the higher frequency, but, because these vortices are not uniformly coherent, the PSD amplitude is substantially smaller. The Strouhal numbers (based on D_s and U_s) corresponding to these frequencies are 0.68 and 1.37. The vortices that emerge from the swirler follow a helical path as they flow downstream. As these paths cross an x-r plane, the vortex cross-section will become clearly visible in the PIV images (see Fig. 9). PSDs of both axial and swirl velocities taken further downstream confirmed the common origin of the vortex patterns in x-r and r-θ planes, since precisely the same dominant frequencies as noted at swirler exit were observed. The presence of these structures in the inner edge of the swirler shear layer also explains the high turbulence levels observed there as noted earlier.

Instantaneous vector maps were also constructed for the case of no central jet flow. The fuel injector exit r-θ plane images now showed only a 2-vortex pattern, with much less coherence between the vortex structures. The PSD data obtained for this configuration is given in Fig. 12. Two peaks are again visible but at half the frequencies observed earlier, which is entirely consistent with the 2-vortex pattern observed. Since the vortex coherence is much weaker, this leads to the increased width of the coherent peaks as the energy in the periodic motion blends into the background turbulence. It should also be noted in Fig. 12 that there is significant energy at a low frequency of around 1Hz, in stark contrast to the PSD shown in Fig. 11 with the central jet flowing. This is evidence of the very strong PVC noted

above in the case without central jet. Confirmation that this was a precession phenomenon was obtained by monitoring the position of the instantaneous vortex centre from the PIV r-θ plane data. These images showed that the vortex core centre was not fixed on the geometric centre-line. Fig. 13 presents the angular position of the instantaneous vortex centre as a function of time. The saw-tooth curve fitted to the data indicates a precession frequency of 0.8 Hz. This confirms the conclusion drawn from the PSD data. The implied Strouhal number of the precession (0.018) agrees well with earlier data on vortex precession given by Syred et al (1994) at this level of swirl number.

CONCLUSIONS

A detailed experimental study using the PIV technique has been carried out of the near-field aerodynamics of a generic high swirl fuel injector configuration. In order to obtain accurate turbulence statistics from the PIV method, validation measurements at different fields of view (FoV) were necessary. Detailed flowfield analysis of both x-r and r-θ plane instantaneous images allowed identification of one cause of apparent high turbulence levels in jet shear layer and centre-line regions. These were connected to a rotating discrete vortex pattern issuing from the fuel injector, and a precessing vortex core respectively. The data set gathered represents a challenging test case for Large Eddy Simulation methods being developed for fuel injector flows.

ACKNOWLEDGEMENTS

The work reported here has been carried out within the UTC in Combustion Aerodynamics at Loughborough University. Funding was provided by an EU FP 5 grant under contract 'MOLECULES' (G4RD-CT-2000-00402).

REFERENCES

Adrian, R. J., 1991, "Particle imaging techniques for experimental fluid mechanics", *Ann Rev of Fluid Mechs*, 23, 261-304.

Anacleto, P. M., Fernandes, E.C., Heitor, M.V., Shtork, S.I., 2001, "Characteristics of a precessing vortex core in an LPP combustor model", *Proc of 2nd TSFP Conf*, Sweden.

Brooke-Benjamin, T., 1962, "Theory of the vortex breakdown phenomenon", *Jnl of Fluid Mechs*, 14, 593-628.

Hollis, D., Spencer, A., Carrotte, J. F., 2001, "Statistical analysis and comparison of LDA and PIV measurements for the flow over a wall-mounted obstacle", *Proc of 9th Int Conf on Laser Anemometry Adv and Apps*, Limerick, Ireland.

Host-Madsen, A., Neilson, A. H., 1998, "Accuracy of PIV measurements in turbulent flows", *Proc of 7th European Symp on Particle Characterisation*, Nurnberg, Germany.

Keane, R. D., Adrian, R. J., 1992, "Theory of cross-correlation analysis of PIV images", *App Scientific Research*, 49, 223-241.

LaVision GmbH, 2000, "PIV Flowmaster Manual".

Leibovich, S., 1978, "The structure of vortex breakdown", *Ann Rev of Fluid Mechs*, 10, 221-246.

Stone, C., Menon, S., 2002, "Open-loop control of combustion instabilities in a model gas-turbine combustor", *Proc of 5th Int Symp on Eng Turbulence Modelling and Measurements*, Elsevier Press, 895-906.

Syred, N., O'Doherty, T., Froud, D., 1994, "The interaction of the precessing vortex core and reverse flow zone in the exhaust of a swirl burner", *Proc of I. Mech. E., Jnl of Power and Energy, 208*, 27-36.

Tang, G., Yang, Z., McGuirk, J. J., 2002, "Large Eddy Simulation of isothermal confined swirling flow with recirculation", *Proc of 5th Int Symp on Eng Turbulence Modelling and Measurements*, Elsevier Press, 885-894.

Wang, S., Rusak, Z., 1997, "The dynamics of a swirling flow in a pipe and transition to axisymmetric vortex breakdown", *Jnl of Fluid Mechs*, 340, 177-223.

Yazdabadi, P., Griffiths, A. J., Syred, N., 1994, "Investigations into the precessing vortex core phenomenon in cyclone dust separators", *Proc of I. Mech. E., Jnl of Proc Eng* 208, 147-154.

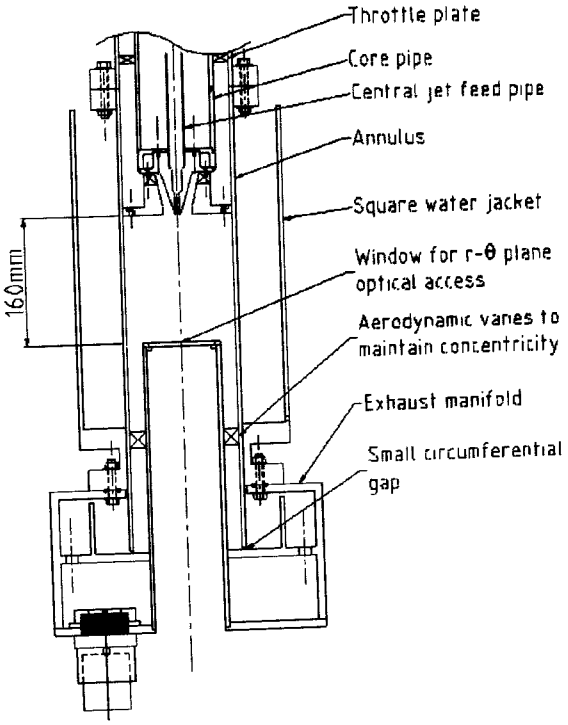

Fig.1 Experimental rig test section.

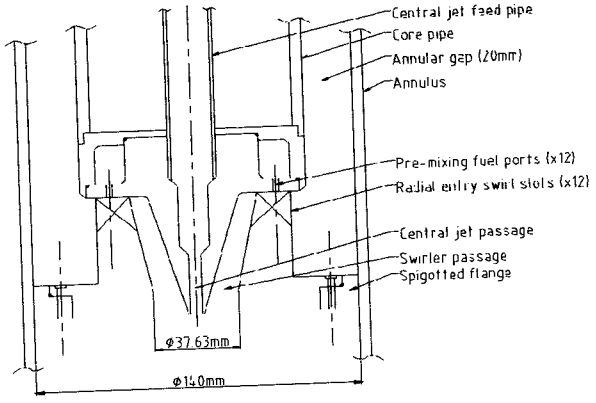

Fig. 2 Fuel injector configuration

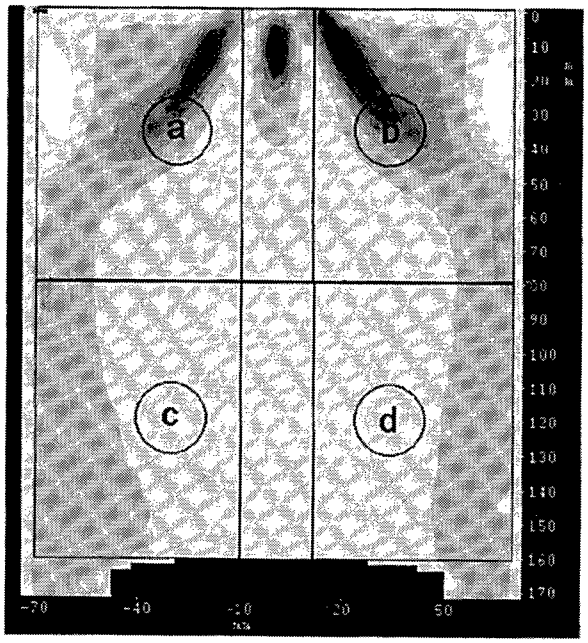

Fig. 3 Large FoV PIV data

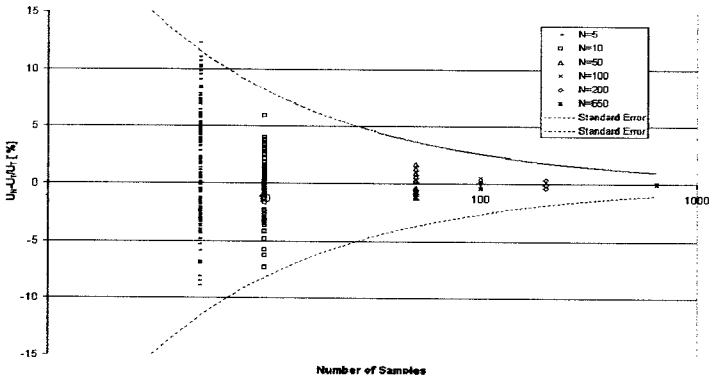

Fig. 4 Statistical convergence of PIV

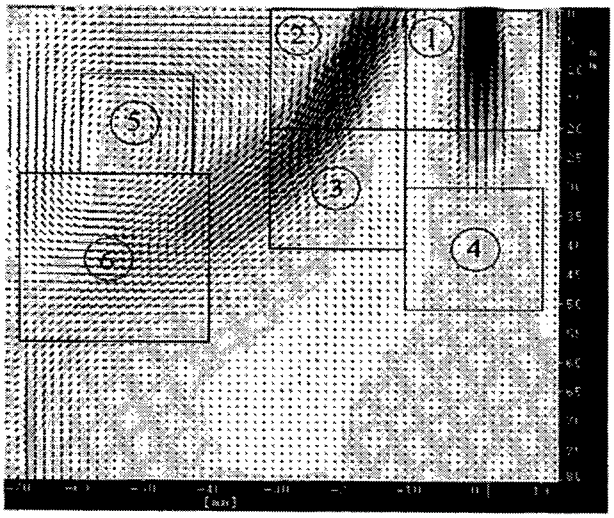

Fig. 5 Intermediate FoV PIV data

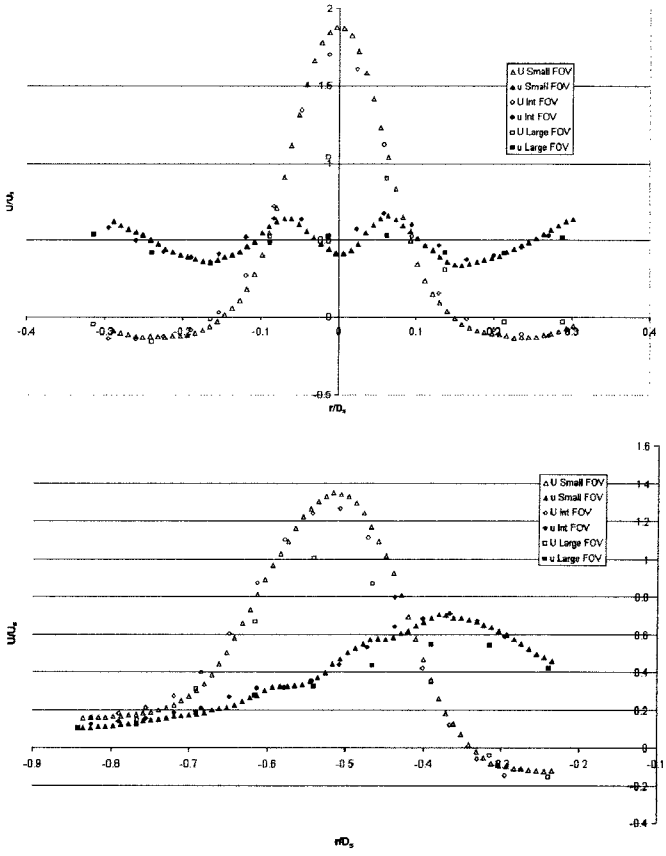

Fig. 6 FoV size comparison at x=10mm
6a (top) jet, 6b (bottom) swirler

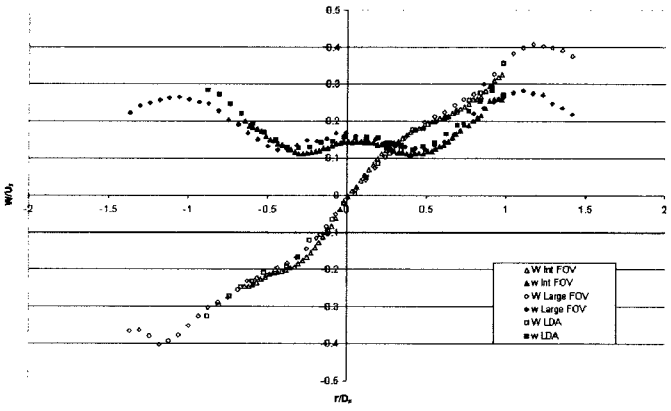

Fig. 7 FoV size and LDA comparison at x = 40mm

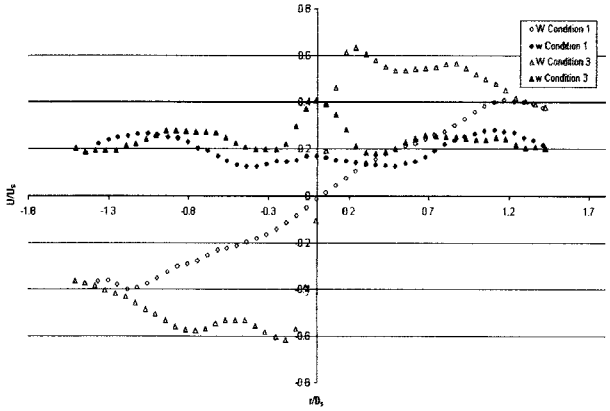

Fig. 8 W mean and r.m.s. at x= 40mm with and without central jet

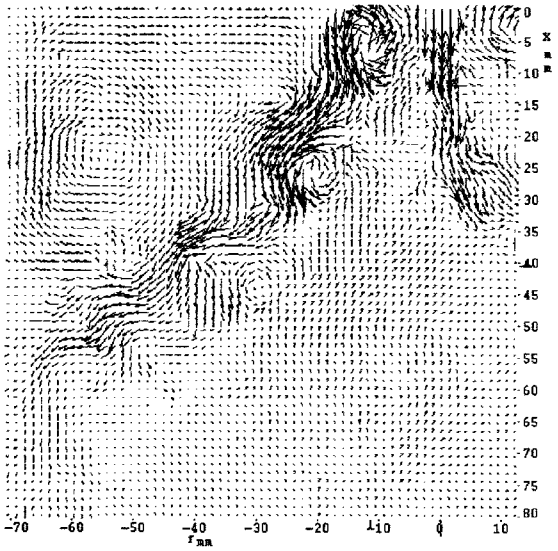

Fig. 9 Instantaneous vector map, x-r plane

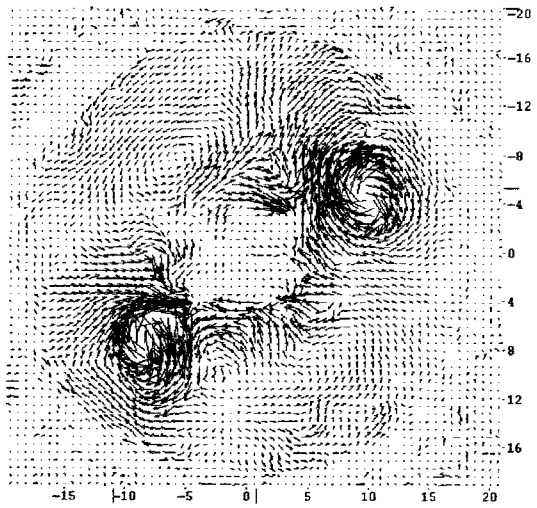

Fig. 10 Instantaneous vector map r-θ plane

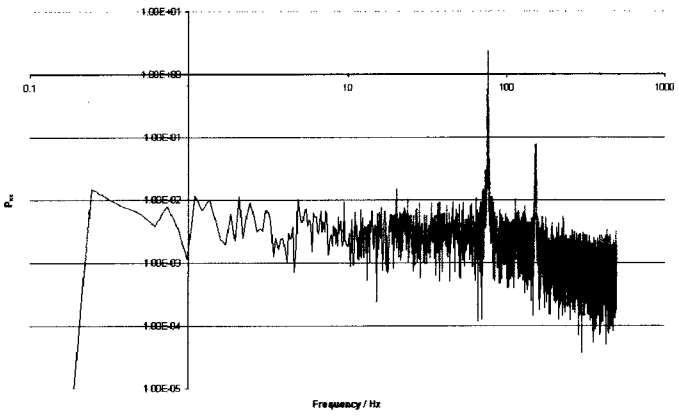

Fig. 11 PSD - W velocity at $x/D_s = 0.03$, $r/D_s = 0.19$

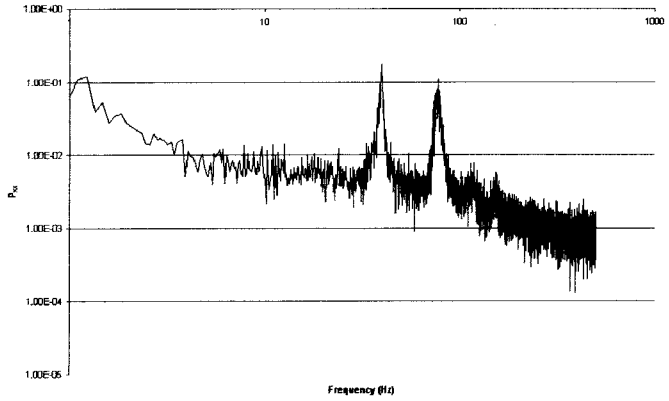

Fig. 12 PSD - W velocity at $x/D_s = 0.03$, $r/D_s = 0.19$ no central jet

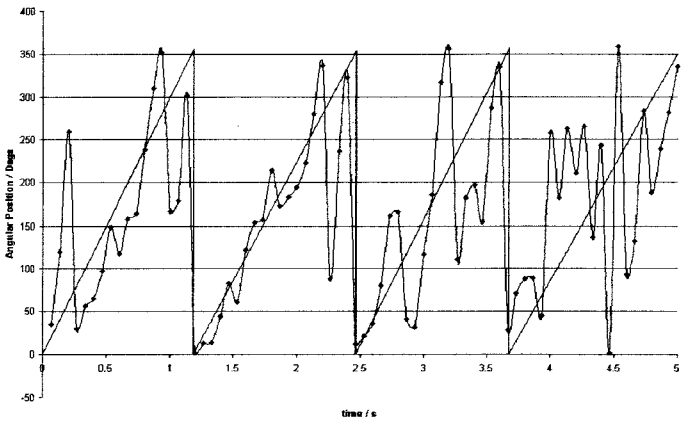

Fig. 13 Position of vortex centre